frontiers | Frontiers in Built Environment

TYPE Original Research
PUBLISHED 23 May 2024
DOI 10.3389/fbuil.2024.1393882

OPEN ACCESS

EDITED BY
Augusto Cesar Da Silva Bezerra,
Federal Center for Technological Education of Minas Gerais, Brazil

REVIEWED BY
Tao Ma,
Southeast University, China
Jianjun Lin,
Yanshan University, China

*CORRESPONDENCE
Min Xiao,
202210184034@mail.scut.edu.cn

RECEIVED 29 February 2024
ACCEPTED 10 April 2024
PUBLISHED 23 May 2024

CITATION
Qiu P, Wang H, Wang P, Xiao M and Wei J (2024), Effects of rock types and crushing mechanism on the 3D morphological parameters of manufactured sands: a combination study of 3D scanning and spherical harmonic analysis.
Front. Built Environ. 10:1393882.
doi: 10.3389/fbuil.2024.1393882

Effects of rock types and crushing mechanism on the 3D morphological parameters of manufactured sands: a combination study of 3D scanning and spherical harmonic analysis

Peiyun Qiu[1], Huaizhi Wang[1], Peng Wang[1], Min Xiao[2]* and Jiangxiong Wei[2]

[1]Guangzhou Metro Construction Management Co., Ltd., Guangzhou, China, [2]School of Materials Science and Engineering, South China University of Technology, Guangzhou, China

This study aims to investigate the effect of rock types, i.e., granite, conglomerate rock, limestone, and crushing mechanism, i.e., Vertical Shaft Impact (VSI) crusher, Horizontal Shaft Impact (HSI) crusher, on the morphology of manufactured sands. By combining the 3D scanning and spherical harmonic analysis, the morphological parameters of manufactured sands such as elongation ratio (*EL*), flatness ratio (*FI*), aspect ratio (*AR*), edge angle (*EA*), sphericity (*SH*), and fractal dimension were quantified. The results indicate limestone is more readily broken into blade-shaped particles without being able to blunt sharp edges through constant abrasion. The proportion of bladed particles in manufactured sand prepared from limestone is 1.91 times higher than the proportion of bladed particles in conglomerates. Additionally, the HSI crusher has a more significant effect on rocks with smaller strength. For the same parent rock, manufactured sand from a VSI crusher contains 30% more spherical and oblate particles than from an HSI crusher.

KEYWORDS

manufactured sand, spherical harmonic analysis, morphological parameter, rock type, crushing mechanism

1 Introduction

Natural sand is an unsustainable exploited and nonrenewable resource, as the main raw material for concrete preparation, approximately 51.7 billion metric tons of natural sand were used annually in industrial construction alone (Kurad et al., 2017; Barry et al., 2023). However, due to the uneven distribution of resources and limited local mining, the supply of natural sand was seriously insufficient. To deal with this problem, many researchers and engineers used manufactured sand as the alternative fine aggregates in concrete constructures (Feng et al., 2018; He et al., 2019; Li et al., 2021; Tawfek et al., 2023). The annual consumption of manufactured sand in the Great Britain and United States of America is estimated to be 230 million tons and 1.73 billion tons respectively (Kankam et al., 2017).

The manufactured sand is generally obtained by crushing rock using mechanical force, which could cause problems of high content of flaky particles, poor particle shape, and strong angularity of the manufactured sand (Aragão et al., 2016; Zhang et al., 2023). Many studies indicated that the manufactured sand with multi-angular shape properties affects the properties of concrete, such as rheology (Hafid et al., 2016), workability (Estephane et al., 2019), and mechanical properties (Felekoğlu, 2007; Wang et al., 2014; Xu et al., 2024). Hence, it is important to control the three-dimensional morphological parameters of manufactured fand. Generally, the properties of manufactured sand are affected by the rock type and the crushing mechanism (Donza et al., 2002; Jamkar and Rao, 2004; Singh et al., 2013). By using image analysis techniques, Hafeez et al. (Hafeez et al., 2016) found that the aggregates obtained by using the cone crusher show higher cubical than those from the jaw crusher. Also by using the image analysis technique, Kamani et al. (Kamani and Ajalloeian, 2020) compared the aggregate shape characteristics produced by common rock types and crushers, and found that the effect of crusher type on aggregate shape characteristics is more in marble and less in tuff. Therefore, capturing the morphological characteristics of manufactured sand and evaluating the effects of rock types and crushing mechanisms on the morphological characteristics are important issues for the production and application of manufactured sand.

The study of sand morphology originated from two dimensions and gradually developed into three dimensions (Zhu et al., 2014). Digital image processing is a traditional method to capture the two-dimensional morphology features of particles (Koohmishi and Palassi, 2017; Ding et al., 2019). For example, Ruan et al. (Ruan et al., 2019) extracted geometric data of 4407 real particles using digital image processing and investigated the effect of particle morphological parameters on the durability of concrete. The result showed that the particle aspect ratio plays a crucial role in the chloride ion diffusion. However, digital image processing cannot accurately represent the three-dimensional (3D) morphology of particles, which results in the obtained conclusions not being representative (Matsumura et al., 2023). Sun et al. (Sun et al., 2014) found that the latter would underestimate sphericity by comparing the 3D true sphericity and the corresponding two-dimensional (2D) sphericity obtained using digital image processing. In recent years, the development of methods such as 3D scanning and X-ray tomography have provided powerful tools for obtaining the 3D morphology of particles. (Li et al., 2022; Wu et al., 2022). These methods have shown very excellent accuracy in particle morphology characterization, especially when solving three-dimensional problems. However, the disadvantages of these methods such as being expensive, and time-consuming also limit their widespread utilization (Wei et al., 2013).

In response to the above problems, scholars have proposed several mathematical analysis methods aimed at simplifying the raw 3D scan data (Ritchie and Kemp, 1999; Rypl and Bým, 2012; Zhou et al., 2015; Thilakarathna et al., 2021; Wei et al., 2022). Among these, the spherical harmonic (SH) function proposed by Garboczi (Garboczi, 2002) is widely applied due to its high efficiency and adaptability in data simplification. For example, Su et al. (Su and Yan, 2019) reconstructed the 3D morphology of particles using spherical harmonic analysis and summarized a 3D angularity and surface texture characterization method. On the basis, Liang et al. (Liang et al., 2021) compared the surface area and volume of sand particles obtained by X-CT scanning and spherical harmonic analysis, and found that the deviation can be controlled within 3% by adjusting the spherical harmonic series.

According to these studies, the combination of 3D scanning and spherical harmonic analysis is attractive to evaluate the rock types and crushing mechanism on the morphology of manufactured sands, which is rarely reported yet. In the present study, the effects of rock types and crushing mechanisms on the morphology of manufactured sands were investigated. Three rock types, i.e., granite, conglomerate rock, and limestone, and two crushing mechanisms, i.e., Vertical Shaft Impact (VSI) crusher and Horizontal Shaft Impact (HSI) crusher were used. By combining the 3D scanning and spherical harmonic analysis, the 3D morphological parameters of manufactured sand, including elongation ratio, flatness ratio, edge angle, sphericity, and fractal dimension, were extracted and analyzed respectively. This study could provide better insight into quality of manufactured sands produced by different rock types and crushing mechanism.

2 Materials and measurement approaches

2.1 Crushers introduction

Two types of common rock crushers, i.e., VSI crusher and HSI crusher were used in this study. The parameters of crushing process could affect the manufactured sand shape (Bouquety et al., 2007). Therefore, these parameters, including the feed speed, closed side setting, open side setting, and speed of the rotor are considered the same for all samples in this study. Meanwhile, the feed size of parent rock was required to be 70–90 mm.

2.1.1 VSI crusher

The VSI Crusher is a crusher that reduces particle size by impacting aggregates against each other. The rotating table gives centrifugal acceleration to the aggregates and creates collisions with side-poured aggregates, as Figure 1A. Aggregates impact with each other resulting in greater uncertainty in the impact surface, which makes it easier to create square particles. The comminution under such loading condition leads to fracture of either flaky or weak particles by cleavage phenomena, resulting in particles with more isometric shapes and greater integrity (Nikolov, 2002; Gonçalves et al., 2007).

2.1.2 HSI crusher

The HSI Crusher works on impact action and uses a rotating horizontal shaft. The aggregates break by colliding with the hammers on the rotating shaft and are further reduced by impacting the impact plate's jaw, as Figure 1B.

2.2 Materials

In this study, five types of manufactured sands were collected. The types of rocks included granite, conglomerate rock, and

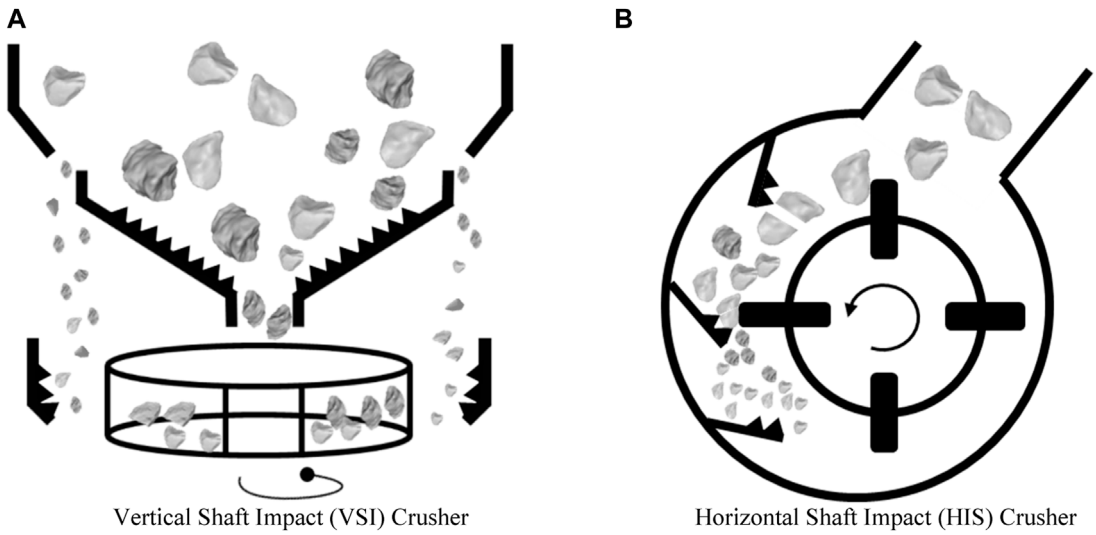

FIGURE 1
Schematic diagram of crusher. **(A)** Vertical Shaft Impact (VSI) Crusher. **(B)** Horizontal Shaft Impact (HIS) Crusher.

TABLE 1 Basic information on manufactured sand.

Name	Source	Parent rock type	Strength (MPa)	Elastic modulus (GPa)	Mineralogy component	Crushing method
VSI-G	Yingde City, Guangdong Province	Granite	123.5	49.6	Feldspar (60%), Quartz (33%)	VSI Crusher
VSI-C	Shaoguan City, Guangdong Province	Conglomerate rock	58.4	13.8	Feldspar (80%), Quartz (15%)	VSI Crusher
VSI-L	Laibin City, Guangxi Zhuang Autonomous Region	Limestone	67.8	10.69	Calcite (90%)	VSI Crusher
HSI-G	Pingnan City, Guangxi Zhuang Autonomous Region	Granite	123.5	49.6	Feldspar (60%), Quartz (33%)	HSI Crusher
HSI-C	Pingnan City, Guangxi Zhuang Autonomous Region	Conglomerate rock	58.4	13.8	Feldspar (80%), Quartz (15%)	HSI Crusher

limestone. Their basic information is shown in Table 1. The photos and grading curves of the manufactured sands obtained are shown in Figure 2 and Figure 3, respectively.

2.3 3D scanning measurement method

As schematically shown in Figure 4, a 3D scanner produced by Guangzhou Electronic Technology Co., Ltd, was used to capture manufactured sand. The resolution of the 3D scanner was set at 0.01 mm to attain an optimal raw point cloud. The main steps are as follows. (1) Sample holding: Fixing the sand by using the playdough. (2) Spraying developer: A white developer was sprayed on the sand surface to ensure scanning quality. (3) Sample Scanning: The upper and bottom halves of sand were scanned in sequence. (4) Data Analysis: The background data were removed, and the upper and lower halves of shell layers were incorporated to obtain a complete surface morphology of the sand. The particle morphology data in *stl* format data were obtained from the 3D scanner after testing, the open-source visualization tool library (VTK, Visualization Toolkit) (Schroeder et al., 2000) was used to read the *stl* format data and converted it to a 3D point cloud x, y, z coordinates and an array of triangular mesh vertices for saving, as shown in Figure 4.

3 3D morphology reconstruction based on spherical harmonic function

In the existing three-dimensional reconstruction methods, a large amount of point data was generated to reconstruct the particle morphology, which resulted in a very inefficient reconstruction of the 3D morphology of manufactured sand. The spherical harmonic function can convert 3D surface data into spherical harmonic coefficients for storage, which greatly reduces the storage space of the data, and has high accuracy and good stability, which is widely used in particle morphology reconstruction (Erdogan et al., 2006; Zhou et al., 2015; Thilakarathna et al., 2021; Wei et al., 2022). Therefore, a voxel-based spherical harmonic

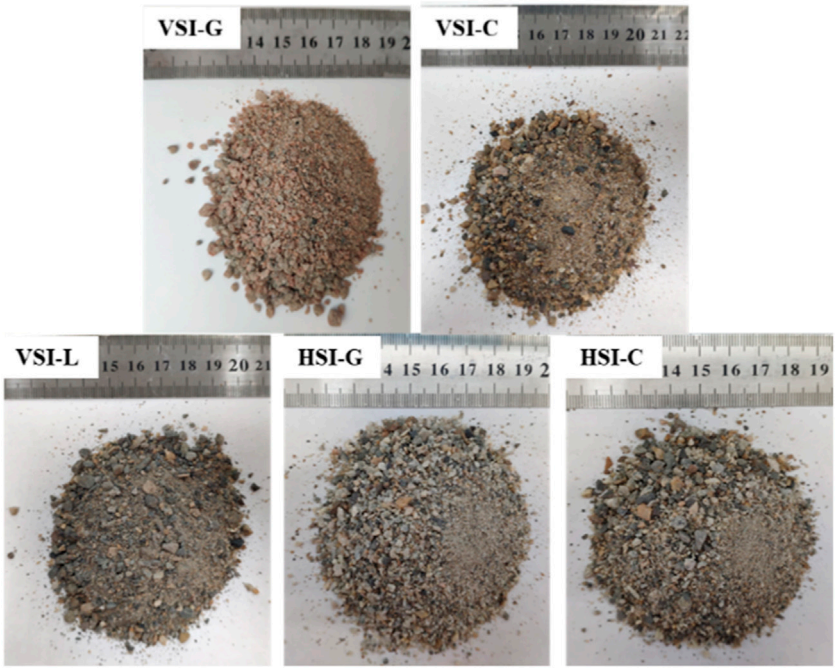

FIGURE 2
Object picture of mechanized sand.

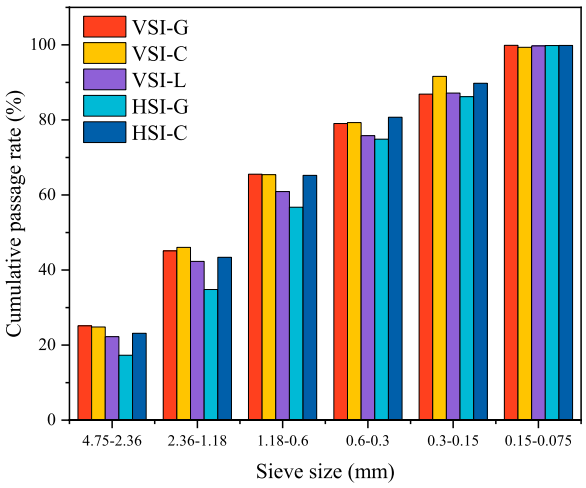

FIGURE 3
Grading curve of manufactured sand.

reconstruction method, was developed by Garboczi et al. (Garboczi and Hrabe, 2020), was applied in the current study. The outline of the procedure is presented in Figure 5. As illustrated in Figures 6A triangular mesh model of manufactured sand was obtained using the 3D scanning measurement method, which is a typical 3D surface model. To facilitate the spherical harmonic transformation, the particle coordinates are converted from a Cartesian coordinate system to a Spherical coordinate system. In contrast, the geometric center of the particle is set as the origin of the spherical coordinate system. The coordination transformation process converts all the triangular mesh vertices to spherical coordinates, as shown in Figure 6B. After obtaining the spherical coordinates, the particle surfaces can be reconstructed using the spherical harmonic function. A detailed description of the spherical harmonic process is given in Supplementary Appendix A. The degree of the SH series (N) in the spherical harmonic function is an important factor affecting the reconstruction accuracy, and a detailed discussion will be shown in Section 5.1.

4 Morphological parameter calculation

4.1 Volume, surface area, and specific surface area

4.1.1 Surface area

The surface of the particle before reconstruction consists of numerous points; after performing the Delaunay triangulation for those, multiple triangular facets used for computing the morphological parameter can be obtained. The surface of the particle after reconstruction was a continuous surface function. Thus, the coordinates of the points corresponding to the scanned locations can be obtained. After performing Delaunay triangulation for the reconstructed points according to the same rules as the scanned points, the triangular facets used for computing the morphological parameter can also be obtained. The reconstruction surface consists of numerous triangular facets, so the surface area can be calculated by using Eq. 1:

$$S = \sum S_i = \sum \frac{1}{2}\left|\overrightarrow{p_1p_2} \times \overrightarrow{p_2p_3}\right| = \frac{1}{2}\left|\overrightarrow{p_1p_2}\right|\left|\overrightarrow{p_2p_3}\right| \sin\theta_1 \quad (1)$$

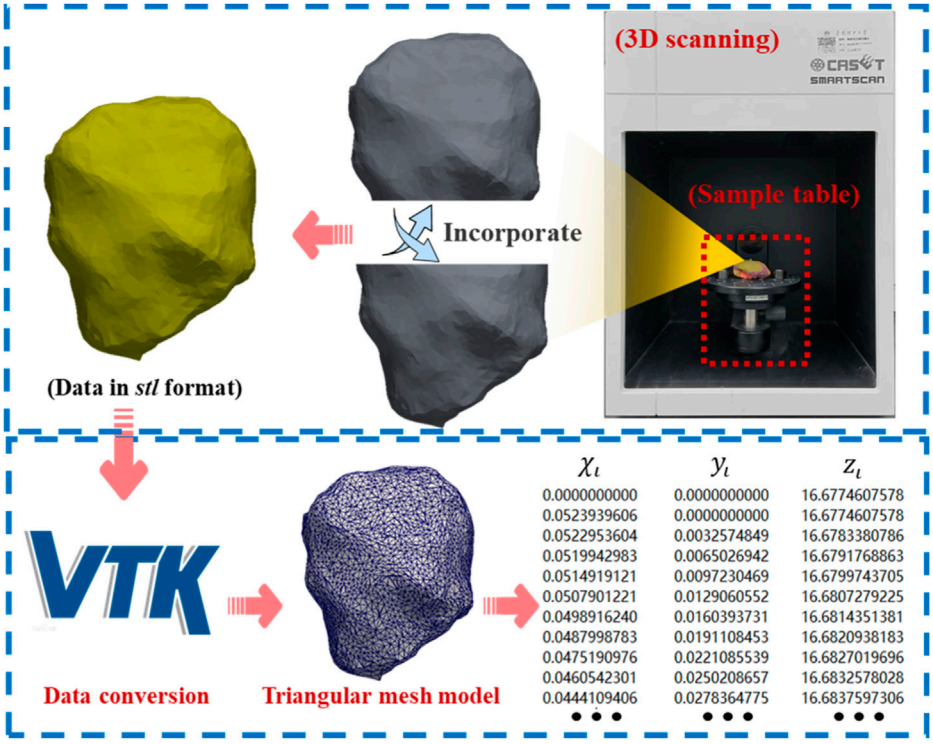

FIGURE 4
Schematic diagram of the three-dimensional scanner and point cloud coordinate extraction.

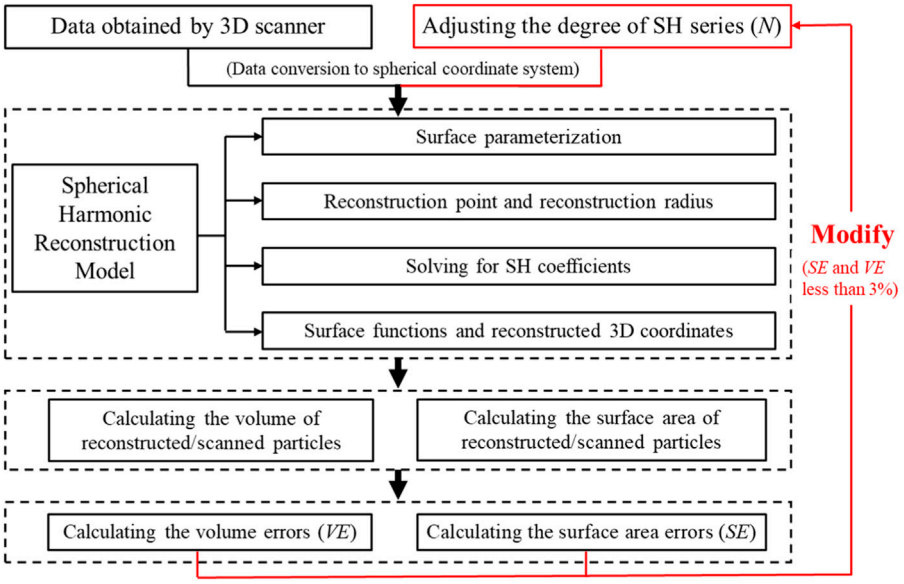

FIGURE 5
Spherical harmonics reconstruction model framework.

where, S is the surface area of particle; S_i is the area of the ith triangular facet; p_1, p_2 and p_3 are the three vertices of each triangular facet, respectively; θ_1 is the angle between vectors and $\overrightarrow{p_2p_3}$.

4.1.2 Volume

As described in Section 4.1.1, the surface of reconstruction particle consists of numerous triangular facets, thus its volume can be calculated by summing the volume of all tetrahedral

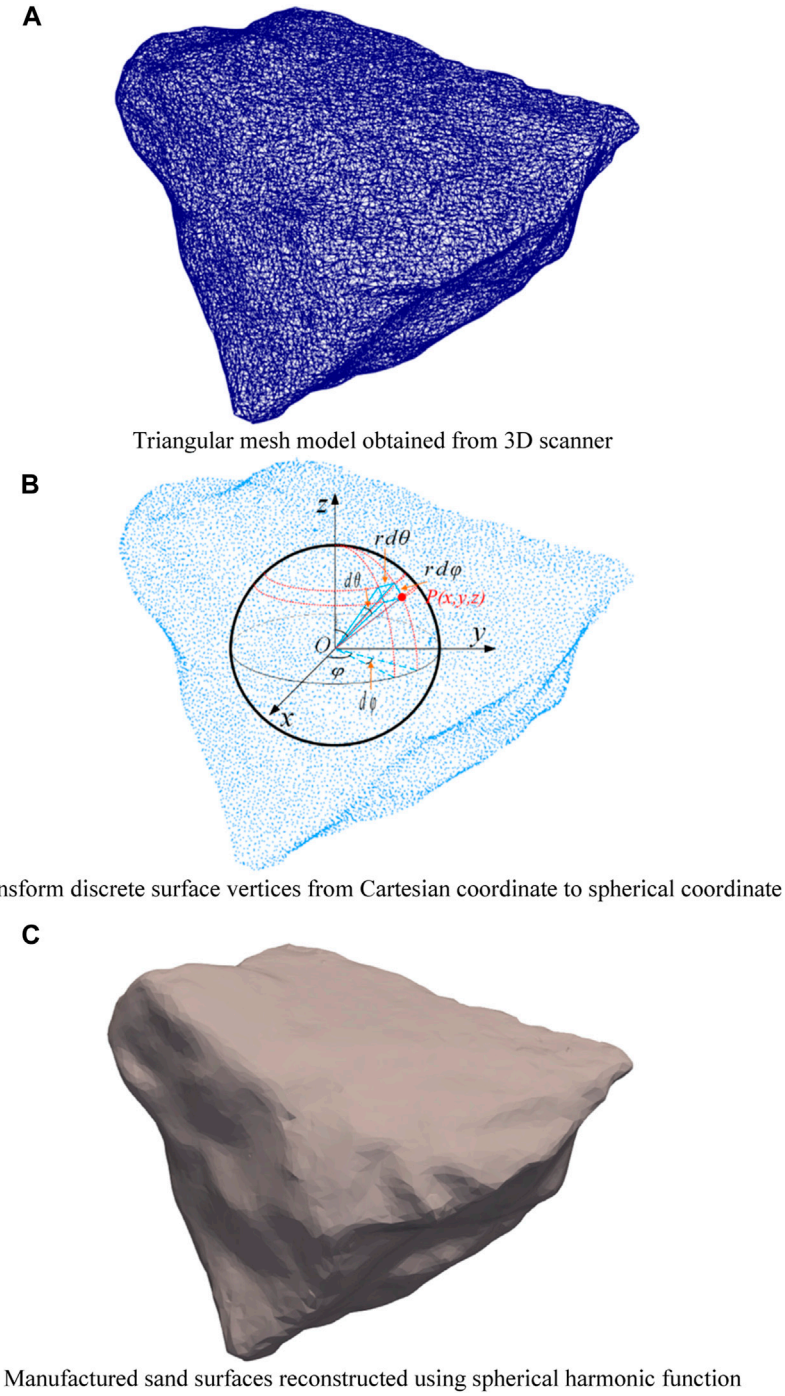

FIGURE 6
Schematic diagram of crusher. **(A)** Triangular mesh model obtained from 3D scanner. **(B)** Transform discrete surface vertices from Cartesian coordinate to spherical coordinate. **(C)** Manufactured sand surfaces reconstructed using spherical harmonic function

formed by the center of particle and the three vertices of each triangular facet, as shown in Eq. 2.

$$V = \sum V_i = \sum \frac{1}{3}\left|OO'\right| \cdot S = \sum \frac{1}{6}\left|\overrightarrow{p_1O} \cdot \left(\overrightarrow{p_1p_2} \times \overrightarrow{p_2p_3}\right)\right| \quad (2)$$

where, V is the volume of the reconstruction shape; V_i is the volume of the ith tetrahedron; S is the Surface area; O is the center of a particle; O' represents the projection of the O at the triangular facet.

4.1.3 Specific surface area

Referring to Ren (Ren et al., 2021), the specific surface area (SSA) of particles was calculated from the surface area and the volume, as shown in Eq. 3.

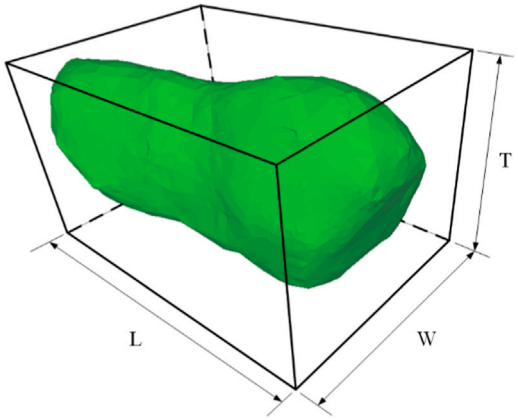

FIGURE 7
Schematic diagram of triaxial size parameters of particles.

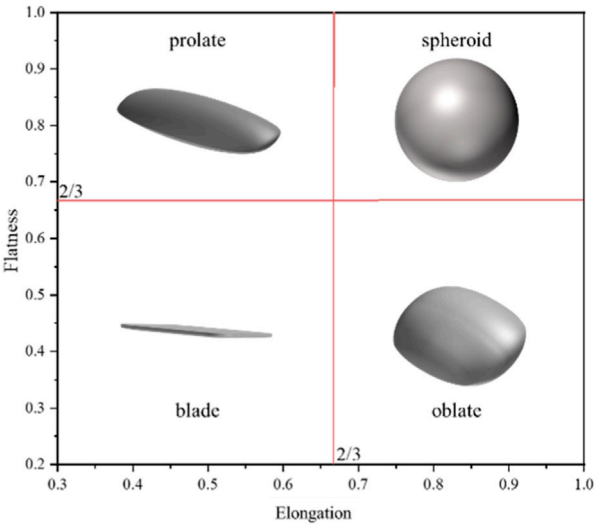

FIGURE 8
Schematic diagram of triaxial size parameters of particles.

$$SSA = \frac{S}{V} \tag{3}$$

where, S is the Surface area of the reconstruction shape; V is the volume of the reconstruction shape.

4.2 Evaluation of reconstruction errors

4.2.1 Volume error

The volume error (VE) was introduced to assess the relative error between the volume calculated from the original point cloud and the volume after reconstruction, as shown in Eq. 4.

$$VE = \frac{|V_0 - V_1|}{V_0} \times 100\% \tag{4}$$

where, V_0 is the volume calculated from the raw point cloud; V_1 is the volume after reconstruction.

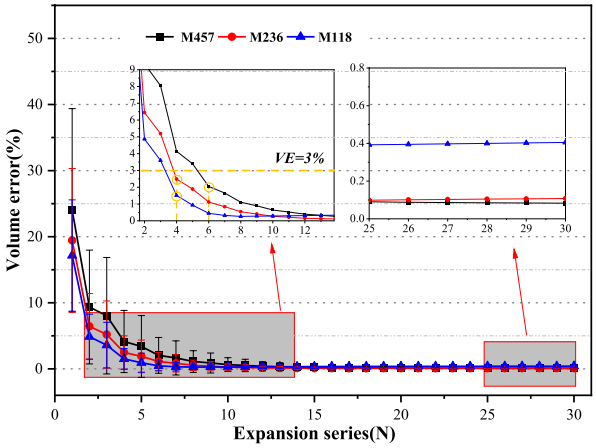

FIGURE 9
Variation of VE with N.

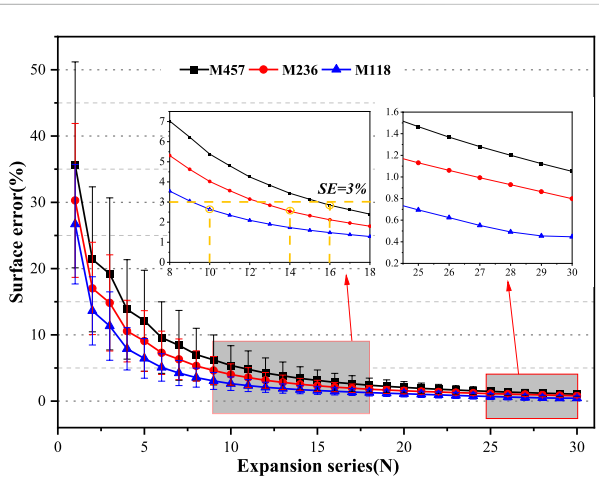

FIGURE 10
Variation of SE with N.

4.2.2 Surface area error

The surface area error (SE) was introduced to assess the relative error between the surface area calculated from the raw point cloud and the surface area after reconstruction, as shown in Eq. 5.

$$SE = \frac{|S_0 - S_1|}{S_0} \times 100\% \tag{5}$$

in which, S_0 is the surface area calculated from the raw point cloud; S_1 is the surface area after reconstruction.

4.3 Three-dimensional morphology characterization

4.3.1 Triaxial size

The three-axis dimensions of the manufactured sand particles are shown in Figure 7, where L, W and T denote the long, middle, and short axes of the manufactured sand particles, respectively.

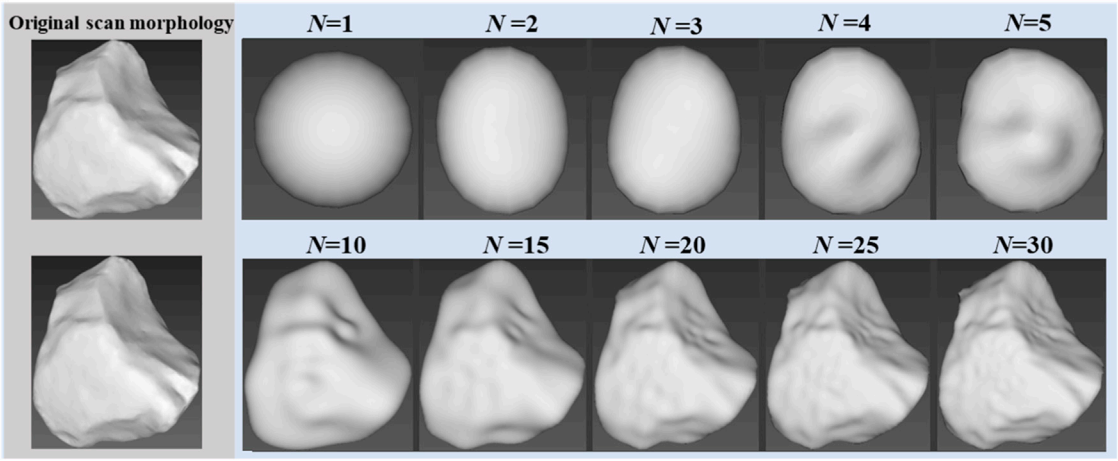

FIGURE 11
Variation of the morphology of particles with *N*.

TABLE 2 The appropriate *N* to achieve a surface area error of less than 3%.

Name	*N* value of M118	*N* value of M236	*N* value of M475
VSI-G	12	15	16
VSI-C	12	14	15
VSI-L	12	15	17
HSI-G	17	18	19
HSI-C	15	18	19

4.3.2 Elongation ratio, flatness ratio, and aspect ratio

Elongation (*EL*)is defined as the ratio of intermediate dimension (*W*) to the longest dimension (*L*), as shown in Eq. 6. Flatness (*Fl*) is defined as the ratio of shortest dimension (*T*) to the intermediate dimension (*W*), as shown in Eq. 7. Aspect ratio (*AR*) is defined as one-half of the sum of flatness and elongation, as shown in Eq. 8.

Referring to Zingg and Masad et al. (Masad and Button, 2000), the particle morphology can be categorized into four classes, including spheroid, prolate, oblate, and blade by fixed arbitrary ratio of 2/3rd (0.67), as shown in Figure 8. Zingg's classification is widely accepted for shape classification due to its ease of use and simplicity of interpretation when compared with other classification methods.

$$El = \frac{W}{L} \tag{6}$$

$$Fl = \frac{T}{W} \tag{7}$$

$$AR = \frac{El + Fl}{2} \tag{8}$$

4.3.3 Sphericity

Referring to the study of Wadell (Wadell, 1932), sphericity (*SH*) is defined as the degree of approximation of the particle shape to an equal volume sphere, as shown in Eq. 9. The SH value ranges from 0 to 1, with larger SH value indicating that the particle is more like a sphere.

$$SH = \frac{4\pi\left(\frac{3V}{4\pi}\right)^{\frac{2}{3}}}{S} \tag{9}$$

where, *S* is the particle surface area; *V* is the particle volume.

4.3.4 Edge angle

Edge Angle (*EA*) is calculated as shown in Eq. 10.

$$EA = \frac{t^2}{2\pi^2}\sum_{\theta=0}^{\pi/t}\sum_{\varphi=0}^{2\pi/t}\frac{\left|R_{EE} - R_p\right|}{R_{EE}} \tag{10}$$

where, R_{EE} is the radial length of the reconstructed particle with *N* of 0; R_p is the radial length of the particle in the spherical coordinate system; *t* is the step size for dividing the polar and azimuthal angles.

4.3.5 Fractal dimension

The fractal dimension can characterize the complexity of the particle geometry, and the larger the fractal dimension is, the more complex the particle geometry is. The two-dimensional fractal dimension proposed by Mandelbrot (Powers, 1953) was extended to three dimensions to characterize the three-dimensional fractal dimension of particles, as shown in Eq. 11. This is later simplified logarithmically to Eq. 12.

TABLE 3 The results of the morphological parameter of manufactured sands.

Name	Statistics	*EI*	*FI*	*AR*	*SH*	*EA*
VSI-G	Mean	0.7419	0.6892	0.7155	0.8464	0.2006
	Min	0.50	0.33	0.47	0.72	0.09
	Max	0.96	0.99	0.93	0.92	0.41
	Std. D	0.0343	0.0483	0.0227	0.0186	0.0188
VSI-C	Mean	0.7462	0.6904	0.7184	0.8486	0.2036
	Min	0.37	0.26	0.48	0.64	0.09
	Max	0.99	0.99	0.94	0.93	0.52
	Std. D	0.0392	0.0392	0.0098	0.0141	0.0121
VSI-L	Mean	0.7356	0.6155	0.6757	0.8210	0.2524
	Min	0.32	0.16	0.42	0.52	0.07
	Max	0.99	0.99	0.90	0.93	0.60
	Std. D	0.0341	0.0546	0.0112	0.0286	0.0239
HSI-G	Mean	0.6365	0.7040	0.6700	0.802	0.261
	Min	0.42	0.42	0.47	0.72	0.11
	Max	0.84	0.94	0.86	0.91	0.46
	Std. D	0.0456	0.0639	0.0092	0.0093	0.0197
HSI-C	Mean	0.6685	0.7495	0.7100	0.8275	0.209
	Min	0.48	0.53	0.58	0.75	0.15
	Max	0.86	0.94	0.79	0.87	0.33
	Std. D	0.0368	0.0095	0.0232	0.0057	0.0103

Note: *EI*, *FI*, *AR*, *SH*, and *EA* represent elongation ratio, flatness ratio, aspect ratio, edge angle, and sphericity, respectively.

TABLE 4 The summary of Student's t-test (*p*-value) for comparing the effect of rock type on the particle morphological.

Sample code	*EI*		*FI*		*AR*		*SH*		*EA*	
	p-value	Sig	*p*-value	Sig	*p*-value	Sig	*p*-value	Sig	*p*-value	Sig
VSI-G and VSI-C	0.707	No	0.069	No	0.203	No	0.973	No	0.379	No
VSI-G and VSI-L	0.762	No	**<0.001**	**Yes**	**<0.001**	**Yes**	**<0.001**	**Yes**	**<0.001**	**Yes**
VSI-C and VSI-L	0.420	No	**<0.001**	**Yes**	**<0.001**	**Yes**	**<0.001**	**Yes**	**<0.001**	**Yes**

Note: where, Sig is the significant difference. Yes: If *p*-value < 0.05, significant differences exist; No: If *p*-value ≥ 0.05, significant differences do not exist.
The bolded *p*-value indicates the probability of selecting a sample of extreme cases.

$$\left(\frac{S(\varepsilon)}{\varepsilon}\right)^{\frac{1}{D}} = a_0 \varepsilon^{\frac{(2-D)}{D}} V(\varepsilon)^{\frac{1}{3}} \tag{11}$$

$$ln\, V = \frac{3}{D} ln\, S - ln\, a_0^3 \tag{12}$$

where, S is the particle surface area; V is the particle volume; a_0 is a constant related to the surface shape; D is the particle fractal dimension, ε is the measurement scale.

5 Results and discussion

In this study, the reconstruction errors of manufactured sand under different *SH* series were evaluated, and the appropriate N value was determined to ensure the calculation accuracy of manufactured sand morphology. Then, the effects of rock types and crushing mechanisms on the morphology parameters of manufactured sand were analyzed using statistics.

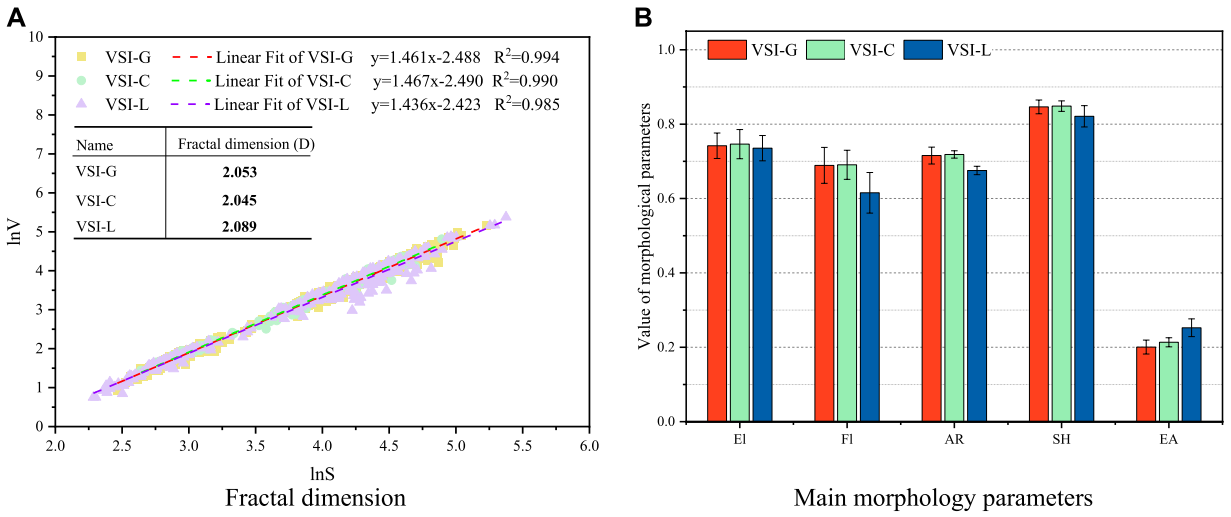

FIGURE 12
Schematic diagram of crusher. **(A)** Fractal dimension. **(B)** Main morphology parameters.

5.1 Verification of reconstruction accuracy

Related studies (Zhou et al., 2015; Su and Yan, 2018) have shown that the degree of SH series has a significant influence on the accuracy of particle reconstruction. A good reconstruction accuracy is achieved when the volume and surface area errors are reduced to less than 3% (Erdogan et al., 2006). In this paper, three different sizes of particles (1.18–2.36 mm (M118), 2.36–4.75 mm (M236), 4.75–9.50 mm (M475)) produced from granite were selected and the number of samples in each group was 30. The *VE* and *SE* of particles were compared with different numbers of *SH* functions (*N*), and a suitable *N* was searched to ensure the credibility of particle reconstruction.

Figure 9 illustrates the variation of *VE* with *N* for different types of particles. For M118, M236, and M475 particles, an *N* of 4, 4, and 6, respectively, is required to have a volumetric error of less than 3%. Meanwhile, as the *N* value is greater than 12, the values of *VE* for all types of particles are essentially stable. Manufactured sand with a larger grain size has more complex edge details.

The variation of *SE* with *N* for different types of particles is like the *VE* vs. *N* curves, as shown in Figure 10. The values of *SE* for all types of particles gradually reduce as the *N* increases. As the same *N* value, the larger the particle size, the greater the *SE* value of particles. For M118, M236, and M475 particles, an *N* of 10, 14, and 16, respectively, is required to have a surface area error of less than 3%. When the *N* value exceeds 25, the surface area error of particles still varies with the *N* value. This is attributed to that the relatively complex surface morphologies on the particle surface have a greater impact on the surface area than the volume, thus a larger *N* is required to reconstruct the surface morphology accurately. This suggests that *SE* than *VE* is more suitable as a control index to determine the suitable *N* value for each kind of particle for ensuring the reconstruction accuracy of particles.

To visualize the change in the morphology of the reconstructed particles with N more intuitively, a reconstructed shape using different *N* was plotted in Figure 11, and the original scanned particle shape was also shown for comparison. As can be seen from Figure 11, when the particle is reconstructed using an *SH* series with a lower *N* (e.g., $N < 10$), the shape of reconstructed particles is relatively mellow due to the low-frequency nature of the low-order *SH* basis functions. This phenomenon leads to the inability of the low-order *SH* series to characterize the angular properties of the manufactured aggregates, thus resulting in a higher *VE* and *SE* (seen in Figure 9; Figure 10). The above analysis shows that the appropriate *N* is essential for ensuring sufficient reconstruction accuracy. Therefore, the appropriate *N* for manufactured sand reconstruction was obtained by requiring *SE* to be less than 3%, and the results are shown in Table 2.

5.2 The effect of rock type on the morphological parameters of manufactured sands

Randomly selected samples of manufactured sand with particle sizes of 1.18–4.75 mm were reconstructed, and the number of samples in each group was more than 80. The morphological parameters of the manufactured sand were calculated concerning the corresponding *N* values in Table 2. The statistical parameters of the manufactured sands are shown according to these sand categories in Table 3. Morphological parameters, including *EI*, *FI*, *AR*, *SH*, and *EA*, can represent the sand form characteristics. Also, statistical parameters, including Mean, minimum (Min), maximum (Max), and standard deviation (Std. D), were shown.

According to Table 3, the *EI* values range from 0.32 to 0.99, *FI* values have a range of 0.16–0.99, and *AR* values are in the range of 0.42–0.94. By comparing the average *EA* and average *SH* values of the manufactured sands prepared from three different rocks, it is found that limestone-manufactured sand (VSI-L) has the largest *EA*, which is 25.8% higher compared to conglomerate-manufactured sand, and limestone manufactured sand (VSI-L) has the smallest *SH*, which is 3% lower compared to conglomerate manufactured sand (VSI-C).

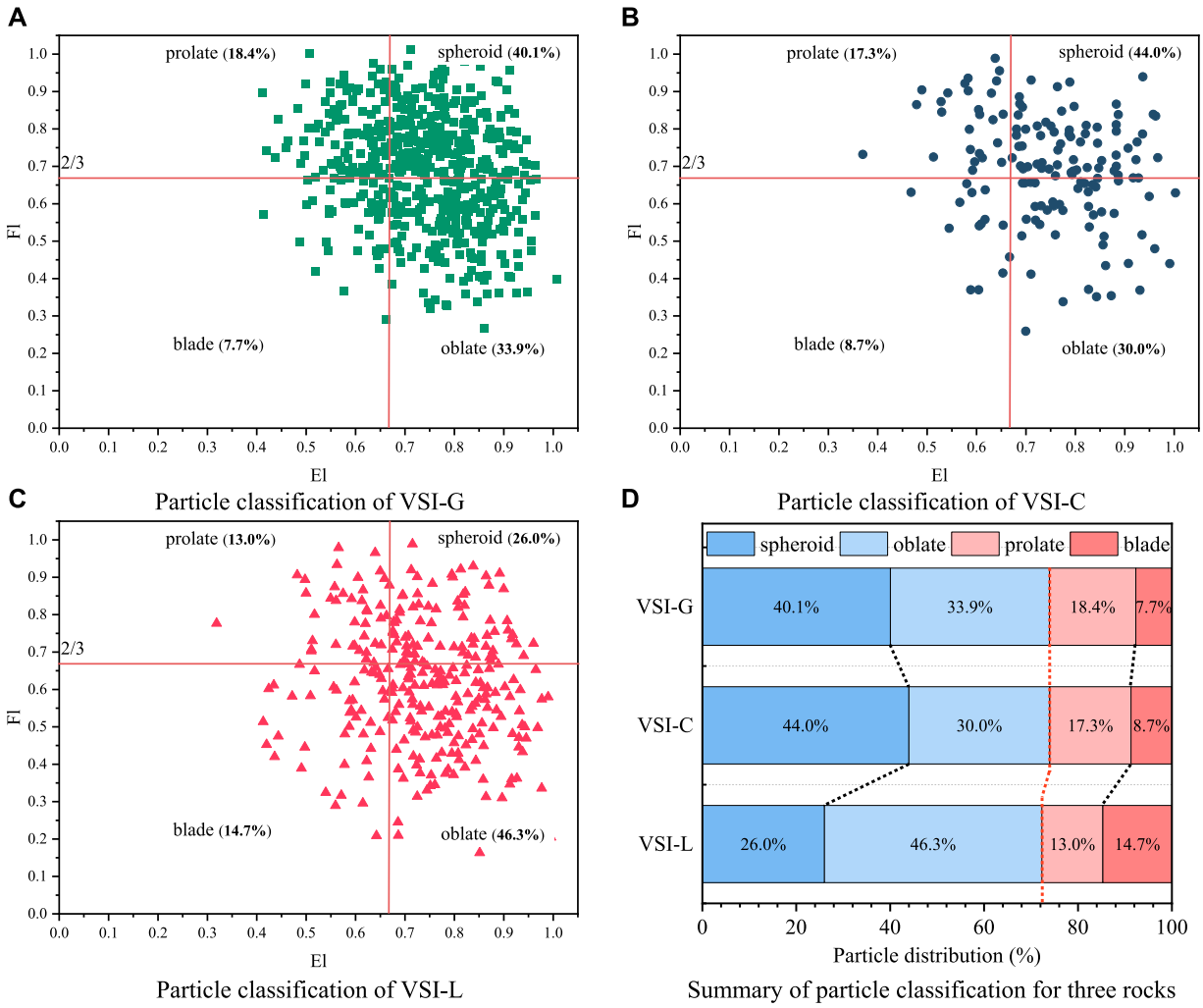

FIGURE 13
Schematic diagram of crusher. **(A)** Particle classification of VSI-G. **(B)** Particle classification of VSI-C. **(C)** Particle classification of VSI-L. **(D)** Summary of particle classification for three rocks.

Meanwhile, there were variations in the morphological parameters of the manufactured sands prepared from different crushers and the same parent rock. For example, the average *SH* of VSI-G is 5.5% larger than that of HSI-G, and the average *SH* of VSI-C is 2.5% larger than that of HSI-C. Similar conclusions were reached comparing the *AR* of mechanism sand from different crushers and the same parent rock. It may show the effects of both parent rock types and crushing mechanisms on the morphology of manufactured sand.

For determining whether the rock type has an essential influence on morphological characteristic parameters of manufactured sands. The Student's t-test for unequal sample sizes was used to assess the statistical significance of the average values of morphological parameters at a significance level of 0.05 (Rouder et al., 2009; Estephane et al., 2019; Chukhrova and Johannssen, 2022). The results of the Student's t-test are shown in Table 4. Comparing manufactured sands prepared with granite (VSI-G) and conglomerate rock (VSI-C), all p was found to be more than 0.05 ($p > 0.05$), indicating that no significant difference existed in the morphology of manufactured sand prepared with granite and conglomerate. Similarly, the multiple comparison analysis indicated that a significant difference existed ($p < 0.05$) in the other combination of the parent rock type (i.e., VSI-G *versus* VSI-L and VSI-C *versus* VSI-L) in morphometric parameters, except for *El*, which was found to be similar.

Figure 12 shows the fractal dimension and average of main morphologic parameters for manufactured sands prepared with three parent rocks (VSI-G, VSI-C, VSI-L). In which, VSI-L has the largest fractal dimension, which is 1.8% larger than that of VSI-C, while the deviation of the fractal dimension between VSI-G and VSI-C is less than 0.4%. It indicates that the geometries of manufactured sand prepared by limestone are more complex and that the morphology of the sand prepared by granite and conglomerate is closer. This is attributed to the similar mineral component of granite and conglomerate. The main morphology parameters of VSI-G and VSI-C also demonstrate identical results. Figure 12B shows that the sphericity of VSI-L is 3.3% smaller than that of VSI-G and VSI-C, while the edge angle is 22.1% larger than that of VSI-G and VSI-C. Limestone is mainly composed of calcite,

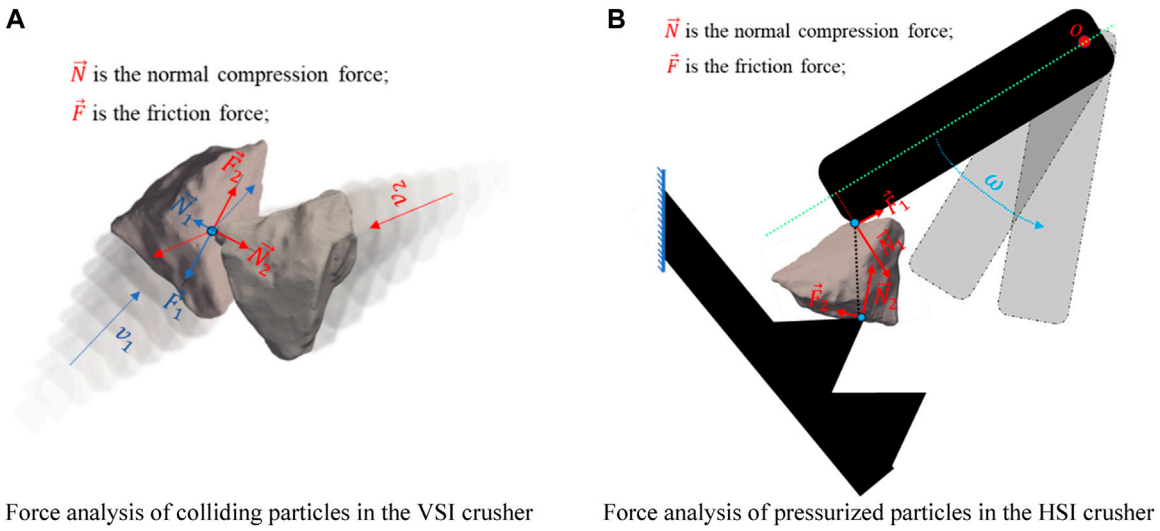

FIGURE 14
Schematic diagram of crusher. **(A)** Force analysis of colliding particles in the VSI crusher. **(B)** Force analysis of pressurized particles in the HSI crusher.

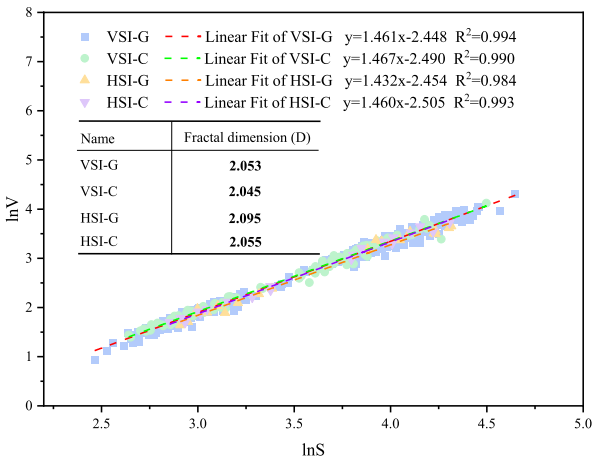

FIGURE 15
Fractal dimension of manufactured sands with different crushing methods.

which has three cleavage planes in different directions and belongs to a perfect cleavage mineral (Jensen et al., 2010) (cleavage rocks are more easily broken up). Limestone is more readily broken into blade-shaped particles without being able to blunt sharp edges through constant abrasion. The key to the nature of the rock type influencing the morphology of manufactured sand lies in its cleavage and surface texture. Similar conclusions were obtained in Mojtaba Kamani's study on rock crushers and rock types affecting aggregate shape (Kamani and Ajalloeian, 2020). As a result, the particle sphericity of manufactured sand prepared from limestone is worse than that of granite and conglomerate under the exact crushing mechanism.

Based on the orthogonal dimension classification method presented by Zingg (Zingg, 1935), the manufactured sand was classified into four classes, including spheroid, prolate, oblate, and blade, as shown in Figure 13. Statistics on the quantity percentage of particles in different classes indicated that VSI-L had least number of particles distributed in spheroid range, only 59.1% of VSI-C. Meanwhile, VSI-L has the highest number of blade particles, reaching 1.91 times VSI-G. This is consistent with the results of the previous analysis on sphericity. It is noticed that VSI-C has 9.7% more particles than VSI-G in the spheroid range. This may be attributed to the fact that conglomerate rock contains more quartz belonging to the non-cleavage mineral (Gao et al., 2021) (non-cleavage rocks are harder broken up), resulting in rocks that may be subjected to more extended periods of abrasion, which is conducive to the formation of more spherical particles. Overall, there are more spherical particles in the manufactured sand prepared with granite and conglomerate compared to limestone.

5.3 The effect of rock crusher on the morphological parameters of manufactured sands

Analyze the typical force condition of rock in the VSI crusher and HSI crusher, as shown in Figure 14. As shown in Figure 14A, the prime crushing mechanism in the VSI crusher is the impact and abrasion of rocks against each other. The mutual abrasion of rocks is conducive to the formation of sub-spherical particles. Therefore, increasing the rock strength may prolong the abrasion time to form better spherical particles. Meanwhile, in the HSI crusher, the rocks are mainly subjected to anvil impact, shear, and friction, as shown in Figure 14B. The shear crushing mechanism tends to produce more sharp particles from the rock surface.

Figure 15 shows the fractal dimension of manufactured sands prepared with different crushing methods (VSI-G, VSI-C, HSI-G, HSI-C). From Figure 15, the fractal dimension of manufactured

TABLE 5 The summary of Student's t-tests (*p*-value) for comparing the effect of rock crusher on the particle morphological.

Sample code	EI		FI		AR		SH		EA	
	p-value	Sig	*p*-value	Sig	*p*-value	Sig	*p*-value	Sig	*p*-value	Sig
VSI-G and HSI-G	**<0.001**	**Yes**	0.993	No	0.077	No	**<0.001**	**Yes**	**0.006**	**Yes**
VSI-C and HSI-C	**0.049**	**Yes**	0.222	No	0.853	No	**0.035**	**Yes**	0.680	No

The p-value indicates the probability of selecting a sample of extreme cases, the exact meaning of which is commented after the table.

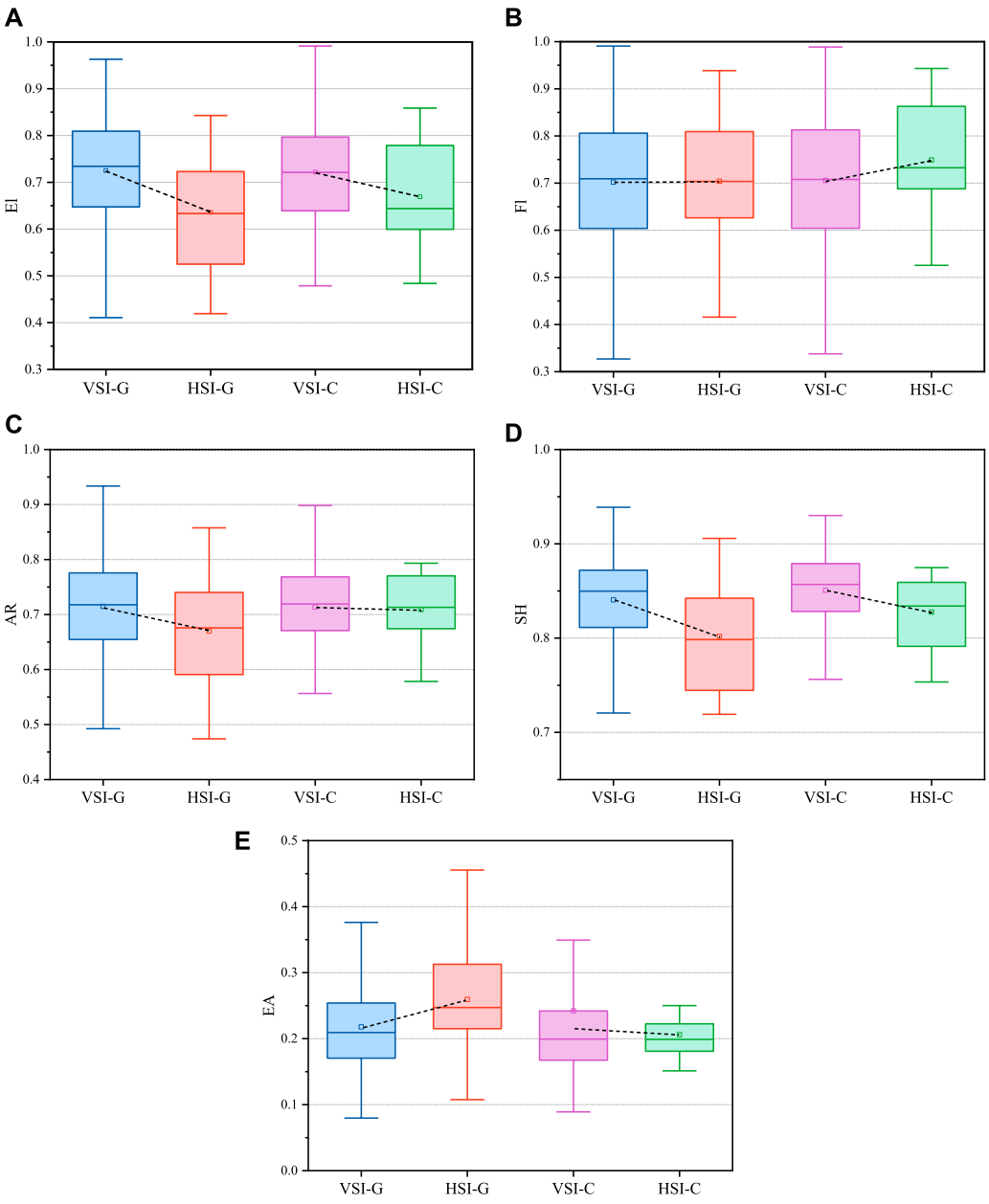

FIGURE 16
Schematic diagram of crusher. **(A)** EI. **(B)** FI. **(C)** AR. **(D)** SH. **(E)** EA.

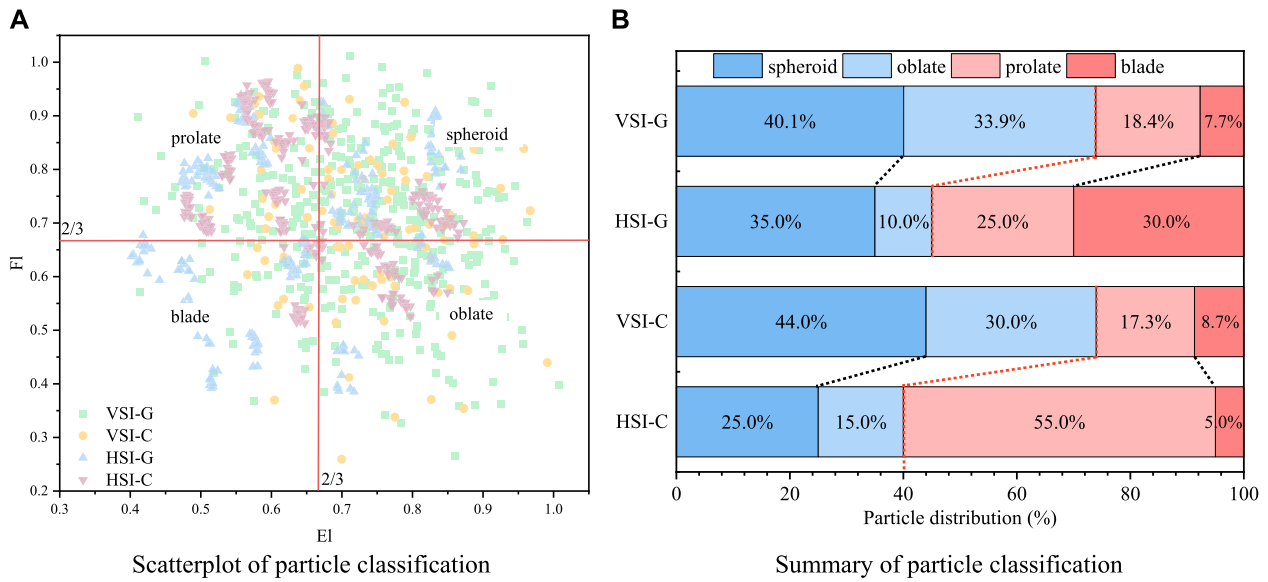

FIGURE 17
Schematic diagram of crusher. **(A)** Scatterplot of particle classification. **(B)** Summary of particle classification.

sands produced from the HSI crusher is higher than sands obtained from the VSI crusher, which indicates that the geometry of the manufactured sand produced by the HSI crusher is more complex.

The Student's t-test was conducted to compare the average morphology parameters of manufactured sand prepared from the VSI crusher and HSI crusher based on the same parent rock, and the results are shown in Table 5. In granite samples, there was a significant difference ($p < 0.05$) in the El, SH, and EA of the manufactured sand produced by the VSI and HSI crushers. However, for the conglomerate, there were few significant differences ($p > 0.05$) in the EA of manufactured sand produced by VSI and HSI crushers, which indicates variability in the effect of crusher type on the different parent rocks.

The boxplot was employed to describe the distribution of the main morphological parameters of manufactured sands, as shown in Figure 16. The boxes contain 50% of the data. Their height values reflect the fluctuation of the data, the line in the box denotes the median value, and the hollow rectangle represents the average value (Liu et al., 2023). Overall, the heights of the pink boxes are all greater than the blue boxes, indicating a more centralized range of distribution of the morphological parameters of the manufactured sand produced by the VSI crusher. This showed similar results in the comparison of VSI-C and HSI-C. The *AR* and *SH* of the manufactured sand produced by the HSI crusher were smaller than those produced by the VSI crusher, indicating that more equi-dimension manufactured sand would be produced using the HSI crusher. For edge angle, HSI-G is 30.1% higher than VSI-G, yet HSI-C and VSI-C are almost identical. This is attributed to the inconsistency of strength between granite and conglomerate. When the strength of the rock is higher, the rock in the HSI crusher breaks up more blade particles under shear, which results in a higher average edge angle in the manufactured sand.

Based on the orthogonal dimension classification method, the shape classification of manufactured sand produced from different crushing mechanisms was carried out, as shown in Figure 17. The VSI crusher produces 74% of manufactured sands in spheroid and oblate, and the overall particle shape tends to be rounded. The manufactured sand made from the HSI crusher has a greater proportion of prolate and blade (55%–60%), and the overall particle shape tends to be flat-long. The VSI crusher produced more sub-spherical particles than the HSI crusher. As a result, the VSI crusher produces better spherical sand for the same rock type than the HSI crusher.

6 Conclusion

This paper extracted morphological parameters of manufactured sand, including *EI*, *FI*, *AR*, *SH*, and *EA*, by combining the 3D scanning and spherical harmonic analysis. Three rock types, i.e., granite, conglomerate rock, and limestone, and two crushing mechanisms, i.e., VSI crusher and HSI crusher, were studied. From the results of this study, the following conclusions can be drawn:

1) The surface area error rather than the volume error is more suitable as a control index to determine the appropriate *N* value for ensuring the reconstruction accuracy of manufactured sand.
2) Rock type significantly affects the 3D morphology parameters of manufactured sand. Notably, well-cleavage rocks are more readily broken into blade-shaped particles without being able to blunt sharp edges through constant abrasion. The proportion of bladed particles in manufactured sand prepared from limestone containing multiple cleavages is 1.91 times higher than in conglomerates.
3) Compared to the HSI crusher, manufactured sand produced with the VSI crusher has a more concentrated distribution of

3D morphology parameters while having a more prominent *SH* and smaller *EA*. For the same parent rock, manufactured sand from a VSI crusher contains 30% more spherical and oblate particles than from an HSI crusher.

In future research, we suggest comparing the effects of combined crushing mechanisms on the morphological parameters of manufactured sand, which is meaningful to further improve the morphological of manufactured sand.

Data availability statement

The original contributions presented in the study are included in the article/Supplementary Material, further inquiries can be directed to the corresponding author.

Author contributions

PQ: Formal Analysis, Investigation, Methodology, Validation, Writing–original draft. HW: Validation, Writing–review and editing. PW: Formal Analysis, Investigation, Methodology, Writing–review and editing. MX: Conceptualization, Supervision, Validation, Writing–review and editing. JW: Supervision, Writing–review and editing.

Funding

The author(s) declare financial support was received for the research, authorship, and/or publication of this article.

Acknowledgments

The authors would like to thank the financial support by the Research on Mechanized Sand Concrete Application Technology for Guangzhou Metro Line 10 (HT211634). The authors would also like to thank Yanfeng Tang for its linguistic assistance during the preparation of this manuscript.

Conflict of interest

Authors PQ, HW, and PW were employed by Guangzhou Metro Construction Management Co., Ltd.

The remaining authors declare that the research was conducted in the absence of any commercial or financial relationships that could be construed as a potential conflict of interest.

Publisher's note

Supplementary material

The Supplementary Material for this article can be found online at: https://www.frontiersin.org/articles/10.3389/fbuil.2024.1393882/full#supplementary-material

References

Aragão, F. T. S., Pazos, A. R. G., Motta, L. M. G. d., Kim, Y. R., and Nascimento, L. A. H. d. (2016). Effects of morphological characteristics of aggregate particles on the mechanical behavior of bituminous paving mixtures. *Constr. Build. Mater* 123, 444–453. doi:10.1016/j.conbuildmat.2016.07.013

Barry, M., Clément, M., Rangeard, D., Jacquet, Y., and Perrot, A. (2023). Manufactured crushed sand: packing fraction prediction and influence on mortar rheology. *Mater. Struct.* 56, 139. doi:10.1617/s11527-023-02231-8

Bouquety, M. N., Descantes, Y., Barcelo, L., de Larrard, F., and Clavaud, B. (2007). Experimental study of crushed aggregate shape. *Constr. Build. Mater* 21, 865–872. doi:10.1016/j.conbuildmat.2005.12.013

Chukhrova, N., and Johannssen, A. (2022). Two-tailed hypothesis testing for the median with fuzzy categories applied to the detection of health risks. *Expert Syst. Appl.* 192, 116362. doi:10.1016/j.eswa.2021.116362

Ding, X., Ma, T., and Huang, X. (2019). Discrete-element contour-filling modeling method for micromechanical and macromechanical analysis of aggregate skeleton of asphalt mixture. *J. Transp. Eng. B-Pave.* 145, 04018056. doi:10.1061/jpeodx.0000083

Donza, H., Cabrera, O., and Irassar, E. F. (2002). High-strength concrete with different fine aggregate. *Cem. Concr. Res.* 32, 1755–1761. doi:10.1016/s0008-8846(02)00860-8

Erdogan, S. T., Quiroga, P. N., Fowler, D. W., Saleh, H., Livingston, R., Garboczi, E., et al. (2006). Three-dimensional shape analysis of coarse aggregates: new techniques for and preliminary results on several different coarse aggregates and reference rocks. *Cem. Concr. Res.* 36, 1619–1627. doi:10.1016/j.cemconres.2006.04.003

Estephane, P., Garboczi, E. J., Bullard, J. W., and Wallevik, O. H. (2019). Three-dimensional shape characterization of fine sands and the influence of particle shape on the packing and workability of mortars. *Cem. Concr. Compos.* 97, 125–142. doi:10.1016/j.cemconcomp.2018.12.018

Felekoğlu, B. (2007). Effects of PSD and surface morphology of micro-aggregates on admixture requirement and mechanical performance of micro-concrete. *Cem. Concr. Compos.* 29, 481–489. doi:10.1016/j.cemconcomp.2006.12.008

Feng, H., Pan, L., Zheng, Q., Li, J., Xu, N., and Pang, S. (2018). Effects of molecular structure of polycarboxylate superplasticizers on their dispersion and adsorption behavior in cement paste with two kinds of stone powder. *Constr. Build. Mater* 170, 182–192. doi:10.1016/j.conbuildmat.2018.02.195

Gao, M., Li, T., Zhu, J., Yin, H., and Yang, Y. (2021). An analysis of relationship between the microfracture features and mineral morphology of granite. *Adv. Civ. Eng.* 2021, 4765731–4765736. doi:10.1155/2021/4765731

Garboczi, E. J. (2002). Three-dimensional mathematical analysis of particle shape using X-ray tomography and spherical harmonics: application to aggregates used in concrete. *Cem. Concr. Res.* 32, 1621–1638. doi:10.1016/s0008-8846(02)00836-0

Garboczi, E. J., and Hrabe, N. (2020). Three-dimensional particle shape analysis using X-ray computed tomography: experimental procedure and analysis algorithms for metal powders. *J. Vis. Exp.* 12, 61636. doi:10.3791/61636

Gonçalves, J. P., Tavares, L. M., Toledo Filho, R. D., Fairbairn, E., and Cunha, E. (2007). Comparison of natural and manufactured fine aggregates in cement mortars. *Cem. Concr. Res.* 37, 924–932. doi:10.1016/j.cemconres.2007.03.009

Hafeez, I., Juniad, F., Kamal, M. A., and Hussain, J. (2016). Influence of single- and two-stage aggregate manufacturing mechanisms on asphalt mixture performance. *J. Mater. Civ. Eng.* 28, 0415180. doi:10.1061/(asce)mt.1943-5533.0001480

Hafid, H., Ovarlez, G., Toussaint, F., Jezequel, P., and Roussel, N. (2016). Effect of particle morphological parameters on sand grains packing properties and rheology of model mortars. *Cem. Concr. Res.* 80, 44–51. doi:10.1016/j.cemconres.2015.11.002

He, H., Wang, Y., and Wang, J. (2019). Effects of aggregate micro fines (AMF), aluminum sulfate and polypropylene fiber (PPF) on properties of machine-made sand concrete. *Appl. Sci.* 9, 2250. doi:10.3390/app9112250

Jamkar, S. S., and Rao, C. B. K. (2004). Index of Aggregate Particle Shape and Texture of coarse aggregate as a parameter for concrete mix proportioning. *Cem. Concr. Res.* 34, 2021–2027. doi:10.1016/j.cemconres.2004.03.010

Jensen, L. R. D., Friis, H., Fundal, E., Møller, P., and Jespersen, M. (2010). Analysis of limestone micromechanical properties by optical microscopy. *Eng. Geol.* 110, 43–50. doi:10.1016/j.enggeo.2009.10.004

Kamani, M., and Ajalloeian, R. (2020). The effect of rock crusher and rock type on the aggregate shape. *Constr. Build. Mater* 230, 117016. doi:10.1016/j.conbuildmat.2019.117016

Kankam, C. K., Meisuh, B. K., Sossou, G., and Buabin, T. K. (2017). Stress-strain characteristics of concrete containing quarry rock dust as partial replacement of sand. *Case Stud. Constr. Mat.* 7, 66–72. doi:10.1016/j.cscm.2017.06.004

Koohmishi, M., and Palassi, M. (2017). Evaluation of morphological properties of railway ballast particles by image processing method. *Transp. Geotech.* 12, 15–25. doi:10.1016/j.trgeo.2017.07.001

Kurad, R., Silvestre, J. D., de Brito, J., and Ahmed, H. (2017). Effect of incorporation of high volume of recycled concrete aggregates and fly ash on the strength and global warming potential of concrete. *J. Clean. Prod.* 166, 485–502. doi:10.1016/j.jclepro.2017.07.236

Li, Y., Qin, X., Zhang, Z., and Dong, H. (2022). Solid waste shape description and generation based on spherical harmonics and probability density function. *Waste Manag. Res.* 40, 66–78. doi:10.1177/0734242x211045003

Li, Y., Zeng, X., Zhou, J., Shi, Y., Umar, H. A., Long, G., et al. (2021). Development of an eco-friendly ultra-high performance concrete based on waste basalt powder for Sichuan-Tibet Railway. *J. Clean. Prod.* 312, 127775. doi:10.1016/j.jclepro.2021.127775

Liang, H., Shen, Y., Xu, J., and Shen, X. (2021). Multiscale three-dimensional morphological characterization of calcareous sand particles using spherical harmonic analysis. *Front. Phys-Lausanne.* 9, 744319. doi:10.3389/fphy.2021.744319

Liu, Y., Zhang, J., Zhao, T., Wang, Z., and Wang, Z. (2023). Reconstruction of the meso-scale concrete model using a deep convolutional generative adversarial network (DCGAN). *Constr. Build. Mater* 370, 130704. doi:10.1016/j.conbuildmat.2023.130704

Masad, E., and Button, J. W. (2000). Unified imaging approach for measuring aggregate angularity and texture. *Comput-Aided Civ. Inf.* 15, 273–280. doi:10.1111/0885-9507.00191

Matsumura, S., Kondo, A., Nakamura, K., Mizutani, T., Kohama, E., Wada, K., et al. (2023). 3D image scanning of gravel soil using *in-situ* X-ray computed tomography. *Sci. Rep-Uk* 13, 20007. doi:10.1038/s41598-023-46772-y

Nikolov, S. (2002). A performance model for impact crushers. *Min. Eng.* 15, 715–721. doi:10.1016/s0892-6875(02)00174-7

Powers, M. C. (1953). A new roundness scale for sedimentary particles. *J. Sediment. Res.* 23, 117–119. doi:10.1306/d4269567-2b26-11d7-8648000102c1865d

Ren, Q., Tao, Y., Jiao, D., Jiang, Z., Ye, G., and De Schutter, G. (2021). Plastic viscosity of cement mortar with manufactured sand as influenced by geometric features and particle size. *Cem. Concr. Compos.* 122, 104163. doi:10.1016/j.cemconcomp.2021.104163

Ritchie, D. W., and Kemp, G. J. (1999). Fast computation, rotation, and comparison of low resolution spherical harmonic molecular surfaces. *J. Comput. Chem.* 20, 383–395. doi:10.1002/(sici)1096-987x(199903)20:4<383::aid-jcc1>3.3.co;2-d

Rouder, J. N., Speckman, P. L., Sun, D., Morey, R. D., and Iverson, G. (2009). Bayesian t tests for accepting and rejecting the null hypothesis. *Psychon. Bull. Rev.* 16, 225–237. doi:10.3758/pbr.16.2.225

Ruan, X., Li, Y., Jin, Z., Pan, Z., and Yin, Z. (2019). Modeling method of concrete material at mesoscale with refined aggregate shapes based on image recognition. *Constr. Build. Mater* 204, 562–575. doi:10.1016/j.conbuildmat.2019.01.157

Rypl, D., and Bým, T. (2012). Geometrical modeling of concrete microstructure for the assessment of ITZ percolation. *Acta Polytech.* 52, 38–47. doi:10.14311/1674

Schroeder, W. J., Avila, L., and Hoffman, W. (2000). Visualizing with VTK: a tutorial. *Ieee Comput. Graph* 20, 20–27. doi:10.1109/38.865875

Singh, D., Zaman, M., and Commuri, S. (2013). Effect of production and sample preparation methods on aggregate shape parameters. *Int. J. Pavement Eng.* 14, 154–175. doi:10.1080/10298436.2011.635792

Su, D., and Yan, W. M. (2018). 3D characterization of general-shape sand particles using microfocus X-ray computed tomography and spherical harmonic functions, and particle regeneration using multivariate random vector. *Powder Technol.* 323, 8–23. doi:10.1016/j.powtec.2017.09.030

Su, D., and Yan, W. M. (2019). Prediction of 3D size and shape descriptors of irregular granular particles from projected 2D images. *Acta Geotech.* 15, 1533–1555. doi:10.1007/s11440-019-00845-3

Sun, Y., Indraratna, B., and Nimbalkar, S. (2014). Three-dimensional characterisation of particle size and shape for ballast. *Géotechnique Lett.* 4, 197–202. doi:10.1680/geolett.14.00036

Tawfek, A. M., Ge, Z., Yuan, H., Zhang, N., Zhang, H., Ling, Y., et al. (2023). Influence of fiber orientation on the mechanical responses of engineering cementitious composite (ECC) under various loading conditions. *J. Build. Eng.* 63, 105518. doi:10.1016/j.jobe.2022.105518

Thilakarathna, P. S. M., Kristombu Baduge, S., Mendis, P., Chandrathilaka, E. R. K., Vimonsatit, V., and Lee, H. (2021). Aggregate geometry generation method using a structured light 3D scanner, spherical harmonics–based geometry reconstruction, and placing algorithms for mesoscale modeling of concrete. *J. Mater. Civ. Eng.* 33, 04021198. doi:10.1061/(asce)mt.1943-5533.0003851

Wadell, H. (1932). Volume, shape, and roundness of rock particles. *J. Geol.* 40, 443–451. doi:10.1086/623964

Wang, J., Yang, Z., and Liu, Y. (2014). Effects of the lithologic character of manufactured sand on properties of concrete. *J. Wuhan Univ. Technology-Mater. Sci. Ed.* 29, 1213–1218. doi:10.1007/s11595-014-1070-9

Wei, D., Zhao, B., and Gan, Y. (2022). Surface reconstruction with spherical harmonics and its application for single particle crushing simulations. *J. Rock Mech. Geotech.* 14, 232–239. doi:10.1016/j.jrmge.2021.07.016

Wei, S., Yiqiang, C., Yunsheng, Z., and Jones, M. (2013). Characterization and simulation of microstructure and thermal properties of foamed concrete. *Constr. Build. Mater* 47, 1278–1291. doi:10.1016/j.conbuildmat.2013.06.027

Wu, M., Wang, J., and Zhao, B. (2022). DEM modeling of one-dimensional compression of sands incorporating statistical particle fragmentation scheme. *Can. Geotech. J.* 59, 144–157. doi:10.1139/cgj-2020-0308

Xu, Y., Chen, H., Liang, Y., Shen, J., and Yang, H. (2024). Study on fracture characteristics and fracture mechanism of fully recycled aggregate concrete using AE and DIC techniques. *Constr. Build. Mater* 419, 135540. doi:10.1016/j.conbuildmat.2024.135540

Zhang, H., Zhao, H., Liu, F., Yang, H., Geng, Y., and Pan, K. (2023). Models for uniaxial stress-strain relationship and thermal properties of fine recycled aggregate concrete exposed to elevated temperatures. *J. Build. Eng.* 66, 105869. doi:10.1016/j.jobe.2023.105869

Zhou, B., Wang, J., and Zhao, B. (2015). Micromorphology characterization and reconstruction of sand particles using micro X-ray tomography and spherical harmonics. *Eng. Geol.* 184, 126–137. doi:10.1016/j.enggeo.2014.11.009

Zhu, Z., Chen, H., Xu, W., and Liu, L. (2014). Parking simulation of three-dimensional multi-sized star-shaped particles. *Modell. Simul. Mater. Sci. Eng.* 22, 035008. doi:10.1088/0965-0393/22/3/035008

Zingg, T. (1935). *Beitrag zur schotteranalyse*. Zürich, Switzerland: ETH Zurich.